

Anyonic interferometry and protected memories in atomic spin lattices

Liang Jiang¹, Gavin K. Brennen², Alexey V. Gorshkov¹, Klemens Hammerer²,
Mohammad Hafezi¹, Eugene Demler¹, Mikhail D. Lukin¹, and Peter Zoller²

¹*Physics Department, Harvard University, Cambridge, MA 02138, USA and*

²*Institute for Theoretical Physics, University of Innsbruck,*

and Institute for Quantum Optics and Quantum Information of the Austrian Academy of Science, 6020 Innsbruck, Austria

(Dated: February 3, 2008)

Strongly correlated quantum systems can exhibit exotic behavior called topological order which is characterized by non-local correlations that depend on the system topology. Such systems can exhibit remarkable phenomena such as quasi-particles with anyonic statistics and have been proposed as candidates for naturally fault-tolerant quantum computation. Despite these remarkable properties, anyons have never been observed in nature directly. Here we describe how to unambiguously detect and characterize such states in recently proposed spin lattice realizations using ultra-cold atoms or molecules trapped in an optical lattice. We propose an experimentally feasible technique to access non-local degrees of freedom by performing global operations on trapped spins mediated by an optical cavity mode. We show how to reliably read and write topologically protected quantum memory using an atomic or photonic qubit. Furthermore, our technique can be used to probe statistics and dynamics of anyonic excitations.

By definition, topologically ordered states [1] cannot be distinguished by local observables, i.e. there is no local order parameter. They can arise as ground states of certain Hamiltonians which have topological degeneracy and which provide robustness against noise and quasi-local perturbations. These properties of such systems are attractive for quantum memories. However, the local indistinguishability makes measuring and manipulating the topological states difficult because they are only coupled by global operations. One way to access this information is to measure properties of the low lying particle-like excitations. In two dimensions, the quasi-particles act like punctures in a surface which can have anyonic statistics and the topological properties are probed by braiding different particle types around each other. The existence of anyons also implies a topological degeneracy [2]. Quantum Hall fluids at certain filling fractions are believed to be topologically protected and there is a vigorous experimental effort to verify anyonic statistics in these systems [3]. A standard approach is to perform some kind of interferometry where one looks for non-trivial action on the fusion state space upon braiding. This is manifested as the evolution of a non-trivial statistical phase in the abelian case, or a change in the amplitude of the participating states in the non-abelian case. Some experimental evidence consistent with observation of abelian anyonic statistics in a $\nu = 2/5$ filled Quantum Hall state has been reported [4] but an unambiguous detection of anyons is still considered an open issue [5].

Spin lattice Hamiltonians can also exhibit topological order and such Hamiltonians can be built with atoms [6] or molecules [7] trapped in an optical lattice. A significant advantage of using atomic systems is that the microscopic physics is well known and there are established techniques for coherent control and measurement. Suggestions have been made for how one would design anyonic interferometers in these systems by using local spin operations to guide excitation along braiding paths [8, 9, 10].

We here present a new approach that directly measures topological degeneracy and anyonic statistics using global operations. The technique involves coupling between a probe qubit (single ancilla spin qubit or optical mode) and topologically ordered atomic spins in an optical lattice. A many body interaction between spins is mediated by coupling to a common bosonic mode of the radiation field via techniques of cavity QED [11, 12, 13, 14] or, alternatively, via a common phonon mode in ion traps [15]. Our approach avoids localizing and guiding excitations while enabling the measurement of the statistical phase associated with arbitrary braiding paths.

We also note that recent experiments have demonstrated braiding operations on small networks of non-interacting qubits encoded in photon polarization [16, 17], which generates a simulation of anyonic interferometry [18]. However, since the background Hamiltonian vanishes in such systems, they are not protected from noise and the particle interpretation of the “excitations” is ambiguous. In contrast, the technique developed here allows one to probe directly dynamic evolution of anyonic quasi-particles within the parent Hamiltonian. In addition, our mechanism can be used to perform reading and writing of qubits initially encoded in light or atoms into topological memory, which may be useful for offline storage during a computation and for applications in long distance quantum communication [19, 20].

ATOMIC AND MOLECULAR SPIN LATTICES IN OPTICAL CAVITIES

We focus on physical systems in which a two-dimensional optical lattice is placed within a high-finesse optical cavity as illustrated in Fig. 2a. To be specific, we consider the 2D square lattice Hamiltonian introduced by Kitaev [21] where each edge of the lattice represents a spin-1/2 particle (see Fig. 1a). Each vertex v or each face f is associated with an

operator $H_v = \prod_{j \in \text{star}(v)} \sigma_j^x$ or $H_f = \prod_{j \in \partial f} \sigma_j^z$. These operators collide on an even number of edges and hence mutually commute. We seek to encode in the $+1$ coeigenspace of these local stabilizers by choosing the so-called *surface-code Hamiltonian*:

$$H_{\text{surf}} = -U \sum_v H_v - J \sum_f H_f. \quad (1)$$

($U, J > 0$). The ground states of H_{surf} have a degeneracy $\dim \mathcal{H}_{g,h} = 2^{2g+h}$ where g is the genus of the surface and h is the number of holes [22]. Designing lattices with genus $g > 0$, such as the surface of a torus, is challenging, but it is possible to create several holes ($h > 0$) in a planar lattice by, for instance, deactivating regions of the lattice with focused far detuned lasers. Alternatively, the planar code with specific boundary as shown in Fig. 1a provides a ground state degeneracy of 2. The logical states are coupled by the operators: $\tilde{Z} = \prod_{j \in C_Z} \sigma_j^z$ and $\tilde{X} = \prod_{j \in C_X} \sigma_j^x$ where the configurations $C_Z(C_X)$ are strings on the lattice (dual lattice) as illustrated in Fig. 1a.

There are several experimental proposals to implement the spin lattice Hamiltonians with topological order. For example, Kitaev's honeycomb lattice Hamiltonian H_{hcb} (see Fig. 1b)[23] can be designed in optical lattices with ultracold atoms using controlled spin exchange interactions [6], or with molecules using microwave induced dipole-dipole interactions [7]. With an appropriate choice of coupling parameters [23], the honeycomb lattice Hamiltonian has a gapped abelian phase with a low energy effective Hamiltonian locally equivalent to H_{surf} . In the following, we will assume the system interacts via H_{surf} , but our results are also applicable to other spin lattice Hamiltonians.

We now consider how to implement the global operations for the spin lattice system. In particular, we are interested in a specific type of global operation: products of Pauli operators on a set of spins whose corresponding edges in the lattice form a connected string. Such global operators are called *string operators*. For example, the generators for the encoded qubits (\tilde{Z} and \tilde{X}) are string operators (see Fig. 1a). All string operators are equivalent to $S_C^z = \prod_{j \in C} \sigma_j^z$ up to local single spin rotations, where C is the set of selected spins. For example, $S_C^x = \prod_{j \in C} \sigma_j^x = \prod_{j \in C} H_j \sigma_j^z H_j$ where H_j is the Hadamard rotation for the j th spin.

In our setup, the topological memory consists of a spin lattice of trapped atoms or molecules inside an optical cavity as illustrated in Fig. 2a. The off-resonant interaction between the common cavity mode and selected spins is described by the quantum non-demolition (QND) Hamiltonian [24, 25]:

$$H = \chi a^\dagger a \sum_{j \in C} \sigma_j^z, \quad (2)$$

which is achieved by choosing the cavity mode with a large detuning Δ from a spin-dependent optical transition as shown in Fig. 2b. The coupling strength is $\chi = g^2/2\Delta$ where g is the single-photon Rabi frequency for the cavity mode. The

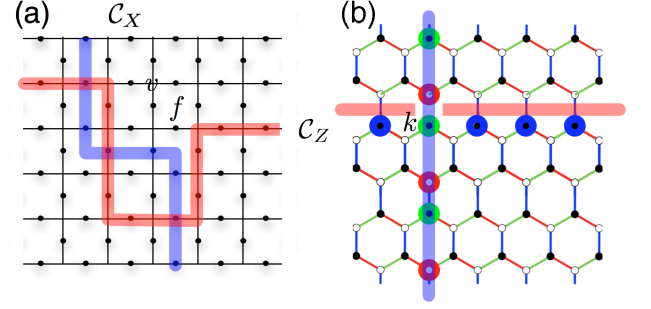


FIG. 1: Generators for the encoded qubits. (a) A planar code which encodes one logical qubit in the ground states. There is a spin-1/2 particle (filled dot) for each edge of the lattice. The interactions of the local Hamiltonian H_{surf} are along edges that bound a face f , and edges that meet at a vertex v . The strings $C_{X,Z}$ indicate paths of products of $\sigma^{x,z}$ operators that are logical operators on the code. (b) A nearest neighbor local Hamiltonian H_{hcb} on the honeycomb lattice, with a spin-1/2 particle for each lattice site. The (green, red, blue) edges represent interactions of type $(\sigma^x \sigma^x, \sigma^y \sigma^y, \sigma^z \sigma^z)$. In the limit that the interactions along the blue links are much stronger than those along the other links, the ground subspace has a gapped \mathbb{Z}_2 topological phase [23]. Physical $(\sigma^x, \sigma^y, \sigma^z)$ spin operations as part of the strings $C_{X,Z}$ are indicated by bold (green, red, blue) circles around the spins. At qubit k , the string crossing, the operation is $\sigma_k^x \sigma_k^z$.

QND Hamiltonian preserves the photon number $n_a = a^\dagger a$ of the cavity mode. In addition, the cavity mode also interacts with an ancilla spin that probes anyonic statistics associated with quasi-particles.

Similar to the previous schemes [8, 10] to measure anyonic statistics, we assume selective addressing of spins in the lattice so that we can perform single spin rotations as well as switch on/off the coupling between the cavity mode and the spins. Such selective manipulation can be achieved using addressing lasers with shaped intensity profiles [26, 27]. The key new ingredient, however, is that we use the common cavity mode to mediate global string operators. In this way, we avoid problems involving maintaining adiabaticity and localization while braiding quasi-particles. And most importantly, we are able to achieve *controlled-string operations* ($\wedge [S_C^{x,z}]$) for an arbitrary string C .

The idea of controlled-string operations can be illustrated by considering a situation when the cavity mode is first prepared in some superposition of zero and one photon states. Within this subspace, the evolution of the QND Hamiltonian for interaction time $\tau = \pi/2\chi$ yields

$$U = \exp[-iH\tau] = \left[(-i)^{N_C} \prod_{j \in C} \sigma_j^z \right]^{n_a} \quad (3)$$

$$= \begin{cases} \mathbf{I} & \text{for } n_a = 0 \\ (-i)^{N_C} \prod_{j \in C} \sigma_j^z & \text{for } n_a = 1 \end{cases},$$

where N_C is the number of elements in C , and the second

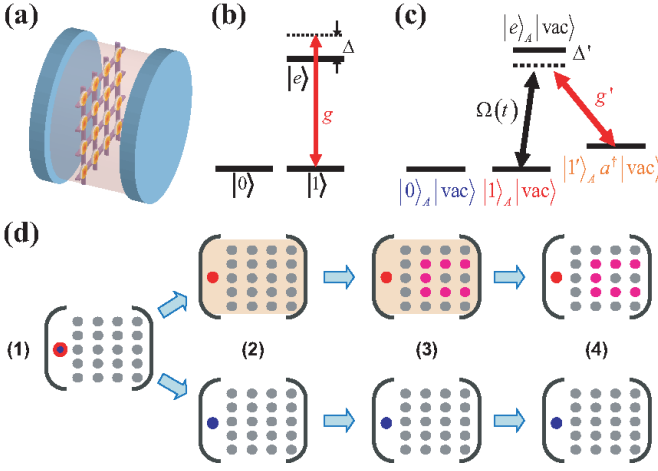


FIG. 2: (a) Inside a cavity, an optical lattice carries spins for topological memory, with individual spin addressability [26, 27]. (b) The energy levels of a selected memory spin interacting dispersively with the cavity mode, which implements the QND Hamiltonian of equation (2). The coupling coefficient is $\chi = g^2/\Delta$, with single-photon Rabi frequency g and detuning Δ . (c) The energy levels of the ancilla spin and the cavity mode for the single photon approach. The control laser $\Omega(t)$ connects the states $|1\rangle_A \otimes |\text{vac}\rangle$ and $|1'\rangle_A \otimes a^\dagger |\text{vac}\rangle$, and enables coherent creation and absorption of a cavity photon conditioned on the ancilla spin. (d) Cartoon illustration of the procedure for the implementation of single-photon approach for controlled-string operations: (1) Initialize the ancilla spin (the left highlighted spin) in a superposition state $\alpha|0\rangle_A + \beta|1\rangle_A$ (blue for $|0\rangle_A$ and red for $|1\rangle_A$), with no photon in the cavity and state $|\psi\rangle_S$ for the topological memory. (2) Coherently create a cavity photon (orange shade) for ancilla spin state $|1\rangle_A$ (upper branch); no photon is created for ancilla spin state $|0\rangle_A$ (lower branch). (3) Switch on the interaction between the cavity photon and the selected spins. If there is a cavity photon (orange shade), a non-trivial evolution S_C^z (pink dots) is implemented. (4) Turn off the interaction and coherently absorb the cavity photon into the ancilla spin. Finally the state $\alpha|0\rangle_A \otimes |\psi\rangle_S + \beta|1\rangle_A \otimes S_C^z |\psi\rangle_S$ is prepared.

equality uses the identity $\exp\left[-i\frac{\pi}{2}\sigma_j^z\right] = -i\sigma_j^z$. This unitary evolution will apply the string operator S_C^z to the topological memory, conditioned on one cavity photon. With such controlled-string operations, we can conveniently access the topological memory, and build anyonic interferometry to probe braiding statistics and dynamics of quasi-particles.

In practice, however, it is actually easier to control the ancilla spin rather than to directly manipulate the photon number state. Therefore, in the following, we will present two approaches to controlled-string operations between the ancilla spin and the topological memory.

CONTROLLED-STRING OPERATIONS

The key operation of the single photon approach is the evolution of the QND interaction described by equation (3). In addition, the cavity mode interacts with a single ancilla spin

using spectroscopically resolvable energy levels as shown in Fig. 2c. Starting with no photon in the cavity mode $|\text{vac}\rangle$ and ancilla spin in state $\alpha|0\rangle_A + \beta|1\rangle_A$, we can coherently couple the number state of the cavity mode with the state of the ancilla spin by adiabatically increasing the Rabi frequency $\Omega(t)$ of the control laser until it is much larger than the single-photon Rabi frequency g' . The intermediate state is then $\alpha|0\rangle_A \otimes |\text{vac}\rangle - \beta|1'\rangle_A \otimes a^\dagger |\text{vac}\rangle$, having the photon number fully correlated with the ancilla spin. Applying the QND interaction with the intermediate state realizes the desired controlled-string operation conditioned on the state of the ancilla spin. Finally, we can reverse the state mapping by adiabatically decreasing the Rabi frequency, which coherently annihilates the photon of the cavity mode and restores the ancilla spin to its logical subspace spanned by $\{|0\rangle_A, |1\rangle_A\}$. Following the procedure summarized in Fig. 2d, we can achieve the controlled-string operation:

$$\Lambda[S_C^z] = |1\rangle_A \langle 1| \otimes S_C^z + |0\rangle_A \langle 0| \otimes \mathbf{I}. \quad (4)$$

The second approach to controlled-string operations is based on the idea of geometric phase gates [28]. Here, the bosonic field of the cavity mode starts in a coherent state, rather than a superposition of zero and one photon states. If our transformation restores the bosonic field to the initial coherent state, the entire system will accumulate a quantum phase (geometric phase), which is twice the area enclosed by the trajectory in phase space of the bosonic field. We activate the geometric phase gate using an ancilla spin which experiences the QND interaction with the cavity mode that can be selectively turned on and off [26, 27]. As illustrated in Fig. 3 and detailed in the Methods section: if the ancilla spin is in state $|0\rangle_A$, the enclosed area vanishes; if the ancilla spin is in state $|1\rangle_A$, the enclosed area has a different sign depending on whether the topological memory is in $+1$ or -1 subspace associated with the string operator S_C^z , yielding again equation (4).

Various imperfections such as photon loss and deviation of the QND interaction can degrade the controlled-string operation. However, we can use a cavity with high Purcell factor P to suppress photon loss [29, 30], and apply quantum control techniques to suppress the deviation of the QND interaction to arbitrarily high order [31, 32]. As derived in the Methods section, the error probability for controlled-string operation is approximately $\sqrt{N_C/P}$, with N_C for the length of the string.

ACCESSING TOPOLOGICAL QUANTUM MEMORY

Controlled-string operations provide an interface between the probe qubit which features easy access and efficient manipulation, and the topological memory which provides good storage. To store quantum states we require two operations: the SWAP_{in} gate which swaps the state of a probe qubit A to memory M initialized in $|\tilde{0}\rangle_M$ and the SWAP_{out} which swaps

back to a probe qubit prepared in $|0\rangle_A$.

$$\begin{aligned}\text{SWAP}_{\text{in}} &= H_A \cdot \Lambda[\tilde{Z}] \cdot H_A \cdot \Lambda[\tilde{X}], \\ \text{SWAP}_{\text{out}} &= \Lambda[\tilde{X}] \cdot H_A \cdot \Lambda[\tilde{Z}] \cdot H_A,\end{aligned}$$

where H_A is the Hadamard gate acting on the probe qubit, and $\Lambda[\tilde{S}]$ represents a controlled-string operation. In addition, universal rotations of the encoded qubit (generally, arbitrary unitaries generated by string operators) over the topological memory can be implemented either by teleportation of quantum gates or by direct geometric phase gate. (See SOM for details.) We remark that the ancilla spin can also be entangled with another ancilla spin from a different cavity via probabilistic entanglement generation, and therefore our topological memories can be used for quantum networks [33, 34, 35, 36, 37].

To compare the topological memory and unprotected single-spin memory, we introduce the decoherence rate q for the unprotected spin due to low-frequency noise. The topological memory can significantly reduce the decoherence rate by a factor of $(\delta h/J)^N \ll 1$, where δh is the magnitude of the noise perturbation on individual spins and N is the length of the minimal string associated with the generators for encoded qubits [21]. Meanwhile, since the topological memory is not protected from errors associated with controlled-string operations (with probability $\sim \sqrt{N/P}$), we should take them into account. Therefore, in terms of total error probability, the topological memory outperforms the single-spin memory for storage time $t \gtrsim \frac{1}{q} \sqrt{N/P}$. (See the Methods section for details).

ANYONIC INTERFEROMETRY

We now describe how to use controlled-string operations to extract the statistical phase acquired when braiding abelian anyons. The definition of anyonic statistics usually relies on the adiabatic transport of quasi-particles around each other [38], with the required condition of adiabaticity to keep the system in the same manifold of excited states and prevent exciting additional degrees of freedom. Note that this procedure relies explicitly on the existence of the Hamiltonian. This is fundamentally different from anyonic simulation approaches [16, 17, 18] not using topological Hamiltonian, which only probe the non-trivial commutation relations of spin operators and initially entangled quantum states. However, anyonic statistics is a property of quasi-particles associated with the Hamiltonian and not just with some specially prepared initial state.

For our spin lattice system with H_{surf} , there are two types of anyons [21]: (1) z-particles that live on the vertices of the lattice and (2) x-particles that live on the face (see Fig. 4a,b). These anyons are created in pairs (of the same type) by string operators: $|\psi^z(l)\rangle = S_l^z |\xi\rangle$ and $|\psi^x(l)\rangle = S_l^x |\xi\rangle$, where $|\xi\rangle$ is some ground state of the spins, and $S_l^z = \prod_{j \in l} \sigma_j^z$ and $S_l^x = \prod_{j \in l'} \sigma_j^x$ are string operators associated with string l on the

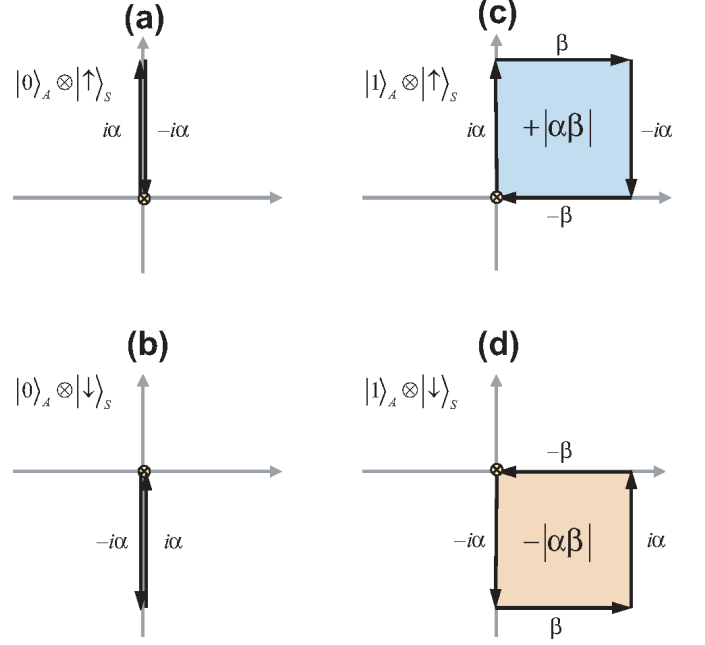


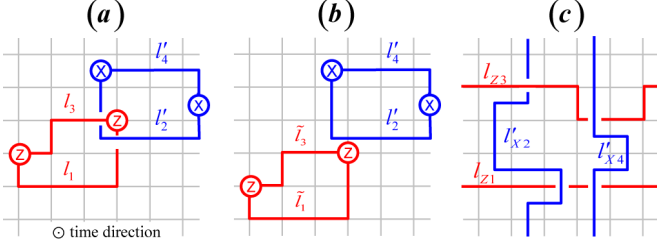
FIG. 3: Phase accumulation for the approach with geometric phase gate [equation (7)]. We use $|\uparrow\rangle_S$ and $|\downarrow\rangle_S$ to represent $+1$ and -1 subspaces of memory spins associated with the string operator S_C^z , respectively. (a)(b) When the ancilla spin is in $|0\rangle_A$ state, the enclosed area vanishes. When the ancilla spin is in $|1\rangle_A$ state, (c) for the subspace $|\uparrow\rangle_S$ the enclosed area is $|\alpha\beta|$; (d) for the subspace $|\downarrow\rangle_S$ the enclosed area is $-|\alpha\beta|$. The quantum phase accumulated is twice the area enclosed.

lattice and string l' on the dual lattice, respectively (see Fig. 4). In our approach, string operators can be used to effectively move quasi-particles quickly along the string trajectory but without exciting other quasi-particles. For example, effective motion of quasi-particles with/without braiding is shown in Fig. 4a,b. This evolution is described by

$$S_{l_4}^x U_{l_3} S_{l_3}^z U_{l_2} S_{l_2}^x U_{l_1} S_{l_1}^z |\Psi_{\text{initial}}\rangle = e^{i\theta_{\text{tot}}} |\Psi_{\text{initial}}\rangle, \quad (5)$$

where we introduce time delays, represented by unitary evolution U_l , between string operations. The goal of these delays is to check that the system stays in the manifold with a fixed number of quasi-particles where time delays lead to only a trivial dynamical phase. On the other hand, if the string operator were to create some complicated intermediate states, time delays would lead to complete decoherence. The total phase $e^{i\theta_{\text{tot}}}$ includes both the dynamical contribution $e^{i\eta} = e^{i2J(t_1+2t_2+t_3)}$ and the statistical contribution $e^{i\theta} = -1$ (or $+1$) in the presence (or absence) of braiding. Therefore, we can unambiguously measure the statistical phase if we can measure $e^{i\theta_{\text{tot}}}$ for both cases.

The following interference experiment can be used to measure the phase $e^{i\theta_{\text{tot}}}$. First, we prepare the probe qubit in a superposition state $(|0\rangle + |1\rangle)/\sqrt{2}$. We then use controlled-string operations to achieve interference of the following two possible evolutions: if the probe qubit is in state $|0\rangle$, no op-



eration is applied to the memory spins; if the probe qubit is in state $|1\rangle$, the operation $S_{l_4}^x U_{l_3} S_{l_3}^z U_{l_2} S_{l_2}^x U_{l_1} S_{l_1}^z$ is applied to the topological memory, which picks up the extra phase $e^{i\theta_{\text{tot}}}$ we want to measure. After the controlled-string operations, the probe qubit will be in state $(|0\rangle + e^{i\theta_{\text{tot}}} |1\rangle)/\sqrt{2}$. Finally, we project the probe qubit to the basis of $|\xi_{\pm}\rangle \equiv (|0\rangle \pm e^{i\phi} |1\rangle)/\sqrt{2}$ with $\phi \in [0, 2\pi)$, and measure the operator $\sigma_{\phi} \equiv |\xi_{+}\rangle\langle\xi_{+}| - |\xi_{-}\rangle\langle\xi_{-}|$. The measurement of $\langle\sigma_{\phi}\rangle$ v.s. ϕ should have fringes with perfect contrast and a maximum shifted by $\phi = \theta_{\text{tot}}$. In fact this scheme can be used to measure abelian statistics for an arbitrary finite cyclic group as described in the Methods section.

It is crucial to verify that the outcome of the anyonic interferometry is invariant under repeated experiments with deformed string operators (see Fig. 4) [39]. For example, the two ground states of the 2D compass model [40] are coupled by perpendicular global X and Z string operators and the phase measured using the interferometry scheme above would also yield a phase -1 due to the anti-commutation relations at the crossing spin. Yet the ground states are not topologically ordered because deformed string operators do not preserve the ground subspace. Since our anyonic interferometry can test all possible braiding operations, we can unambiguously verify the topological property of anyons.

Various imperfections will degrade the signature of anyonic statistics. The string operators may have errors that excite unwanted anyons, and the topological memory may not fully restore to the ground state after braiding. In addition, the topological memory may have anyons from imperfect initialization. If these anyons are enclosed by the braiding loops, they will affect the phase factor associated with braiding. However, neither of these imperfections will prevent us from probing anyonic statistics, since they only reduce the contrast of the anyonic interferometry without shifting the fringes of $\langle\sigma_{\phi}\rangle$. We may even distinguish the two types of imperfections from the contrast that depends on different loops. The reduction of the contrast is proportional to the length of the loops for errors from string operators, while it is proportional to the area enclosed by the loops for errors from imperfect initialization

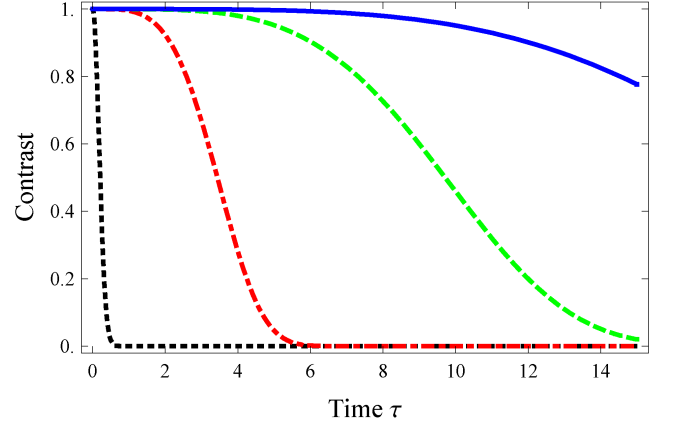


FIG. 5: Fringe contrast of anyonic interferometry as a function of the time for anyonic diffusion. The fringe contrast quickly reduces due to anyonic diffusion (black dotted line). However, we can extend the fringe contrast to longer times by applying one (red dotted-dashed line), four (green dashed line), or ten (blue solid line) pairs of time-reversal operations of U_{π}^z within the time interval τ . For clarity, we only consider the diffusion of two intermediate x-particles induced by the perturbation $h_e^x \sigma_e^x$ from equation (6). We choose the unit of time so that the perturbation strength is normalized $\sqrt{\langle(h_e^x)^2\rangle} = 1$, and we assume that the random field h_e^x is a Gaussian random process with correlation time $\tau_c = 10$. (See SOM for details.)

(see discussion in the Methods section).

PROBING AND CONTROL ANYONIC DYNAMICS

Our anyonic interferometry provides a tool to study the dynamics of anyons. First, consider repeating the protocol [equation (5)] for anyonic interferometry with the time delays $\{t_j\}_{j=1,2,3}$ between the four controlled-string operations. Processes of anyonic creation, propagation, braiding, and annihilation will induce a time dependence of the final state wavefunction in a general expression: $|\Psi_{\text{final}}\rangle = \alpha(\{t_j\})|\Psi_{\text{initial}}\rangle + \beta(\{t_j\})|\Psi_{\perp}(\{t_j\})\rangle$, where $\langle\Psi_{\text{initial}}|\Psi_{\perp}(\{t_j\})\rangle = 0$. Since the reduced density matrix of the probe qubit is $\rho = \frac{1}{2} \begin{pmatrix} 1 & \alpha(\{t_j\}) \\ \alpha^*(\{t_j\}) & 1 \end{pmatrix}$, we can measure the complex coefficient $\alpha(\{t_j\})$ using quantum state tomography [41] of the probe qubit.

Probing anyonic statistics can be regarded as special cases, with $\alpha = e^{i(\theta+\eta)}$ or $e^{i\eta}$, and $\beta = 0$. Although the anyons are immobile for the surface code Hamiltonian, the mobility of quasi-particles may change when we include local perturbations, because the excited states with anyons are highly degenerate and any small perturbation to the Hamiltonian can dramatically change the eigen-wavefunctions. Consider for example a specific diffusion model for anyons induced by the

local perturbation

$$H_{\text{pert}} = \sum_{\alpha \in \{x,y,z\}} \sum_{e \in \text{All spins}} h_e^\alpha \sigma_e^\alpha, \quad (6)$$

where the $h_e^{x,z}$ field components cause diffusion of x(z)-particles and the h_e^y field component causes diffusion of dyonic particles (pairs of neighboring x-particle and z-particle). (See SOM for details). The nature of the perturbation (e.g., time independent or changing with time) determines diffusion dynamics of anyons, which can be observed from the coefficient $\alpha(\{t_j\})$ using our anyonic interferometry.

In addition, we can even control the diffusion dynamics of anyons. We introduce the effective time-reversal operations $U_\pi^z \equiv \prod_{e \in \text{All spins}} \sigma_e^z$ and $U_\pi^x \equiv \prod_{e \in \text{All spins}} \sigma_e^x$, which anti-commute with $h_e^x \sigma_e^x$ and $h_e^z \sigma_e^z$ terms of H_{pert} , respectively. The combination of these operations (e.g., $U_\pi^{\tau/4} \dots U_\pi^{\tau/4} U_\pi^{\tau/4} \dots U_\pi^{\tau/4}$) is analogous to spin-echo pulses in NMR, which can effectively reverse anyonic diffusion caused by static perturbations and consequently extend the fringe contrast of anyonic interferometry to longer time delays, as illustrated in Fig. 5. In essence, by applying these global operations, we can localize the anyons without any trapping potential. (See SOM for details.) Note that the anyonic interferometry is closely related to the Ramsey experiments in atomic physics [42], which can now be performed with anyonic quasi-particles.

OUTLOOK

Controlled-string operations can be applied to other lattice Hamiltonians as well [43, 44], which may provide robust quantum memory with their degenerate ground states. For example subsystem codes [43] can be constructed out of 2D and 3D nearest neighbor spin-1/2 interactions that are realizable with atomic systems [6, 7]. Our approach can be adapted to perform the logical operations generated by strings or planes of Pauli operators in the 2D and 3D subsystem codes, respectively. In addition, the ability to measure global operators on a spin lattice provides a means to probe other properties of topological phases. For example, a class of topologically ordered spin states known as string net states [45], which includes the ground states of H_{surf} , have the property that they are invariant under large closed loop operations. In the present case, these operators are $X_{\text{loop}}(Z_{\text{loop}}) = \prod_{j \in C_{X,Z}^{\text{closed}}} \sigma_j^{x,z}$ which have expectation value 1. A perturbation on H_{surf} in the regime $U \gg J$, by, e.g. a magnetic field, acts like a string tension that reduces the amplitude of large loops (on a vacuum reference state). In fact there are two phases as a function of the strength of the perturbation. For very weak perturbations it has been argued that the loop order parameter scales with the perimeter of the loop while for strong perturbations it scales with the area [46]. These are known as deconfined and confined phases in analogy to lattice gauge theory and are examples of phenomena that could be observed using our protocol. It may also be

interesting to consider adapting the present protocol to spin-lattice systems with non-abelian anyons [47].

METHODS

Derivation of the geometric phase gate

We describe the necessary elements to construct the geometric phase gate illustrated in Fig. 3. First we require the displacement operator $D(\xi) \equiv e^{\xi a^\dagger - \xi^* a}$ that can be obtained by injecting coherent states through cavity mirrors. The amplitude and phase of the injected field determine the phase space displacement of the bosonic field by ξ .

Second, we need the displacement operation that depends on the state of the memory spins:

$$D\left(\alpha e^{i\frac{\pi}{2} S_C^z}\right) = \begin{cases} D(i\alpha) & \text{if } \langle S_C^z \rangle = +1 \\ D(-i\alpha) & \text{if } \langle S_C^z \rangle = -1 \end{cases},$$

where we use $\langle S_C^z \rangle = \pm 1$ to represent the ± 1 subspaces of the memory spins associated with the operator S_C^z . We can achieve $D\left(\alpha e^{i\frac{\pi}{2} S_C^z}\right)$ by applying the QND Hamiltonian for time $t_C = \pi/2\chi$ both before and after the displacement operation $D(\alpha e^{i\phi})$. The justification is based on the identity

$$D\left(\alpha e^{i\phi + i\theta \Lambda}\right) = R(\theta O) D(\alpha e^{i\phi}) R(-\theta O),$$

with $R(x) = e^{ixa^\dagger a}$ and the two commuting operators $[O, a] = 0$. For $O = \sum_{j \in C} \sigma_j^z$ and $\theta = \pi/2$, we have $e^{i\phi + i\theta O} = e^{i\phi} \prod_{j \in C} \exp\left[i\frac{\pi}{2} \sigma_j^z\right] = e^{i(\phi - m\pi/2)} \prod_{j \in C} \sigma_j^z$, with $m = N_C$. Therefore, by choosing $\phi = (m+1)\pi/2$, we obtain $D(\alpha e^{i\theta O + \phi}) = D\left(\alpha e^{i\frac{\pi}{2} S_C^z}\right)$.

Third, we need dispersive coupling between the bosonic field and the ancilla spin (with two levels $\{|0\rangle_A, |1\rangle_A\}$)

$$V_A = \chi_A a^\dagger a |1\rangle_A \langle 1|,$$

with coupling strength χ_A , which can be switched on and off via optical control [26, 27] or mechanical displacement of the ancilla spin. With such dispersive interaction, we are able to obtain the displacement operation conditioned on the state of the ancilla spin, $D(\beta |1\rangle_A \langle 1|) = |0\rangle_A \langle 0| \otimes \mathbf{I} + |1\rangle_A \langle 1| \otimes D(\beta)$, by the following procedure: (1) apply the interaction V_A for time $t_A = \pi/\chi_A$, (2) displace the bosonic field by $-\beta/2$, (3) apply the interaction V_A again for time t_A , and (4) displace the bosonic field by $\beta/2$. The steps (1-3) displace the bosonic field by $\mp\beta/2$ for the ancilla spin in state $|0\rangle_A$ and $|1\rangle_A$, respectively. Combined with the displacement $\beta/2$ from step (4), we have the operation $D(\beta |1\rangle_A \langle 1|)$.

Finally, the controlled-string operation is a combination of the above elements:

$$U = D(-\beta |1\rangle_A \langle 1|) D\left(-\alpha e^{i\frac{\pi}{2} S_C^z}\right) D(\beta |1\rangle_A \langle 1|) D\left(\alpha e^{i\frac{\pi}{2} S_C^z}\right). \quad (7)$$

The bosonic field is restored to its initial state, while accumulating a phase depending on both the state of the ancilla spin and the value for the string operator as illustrated in Fig. 3.

Fidelity of controlled-string operations and topological memory

To evaluate the advantage of using topological memory storage, we compare the improvement of storing a qubit in spins prepared in the ground states of H_{surf} (assumed at zero temperature) versus the decoherence rate for encoding a qubit in a single spin. For long-time storage of quantum memory, we expect to gain from the robustness of the topological memory can significantly reduce the decoherence rate by a factor of $(\delta h/J)^N \ll 1$, where δh is the magnitude of the noise perturbation on individual spins and N is the length of the minimal string associated with the generators for encoded qubits [21]. The controlled-string operations that are used to swap quantum information in and out have errors including cavity decay, radiative decay, and non uniform dispersive shifts in the QND interaction.

Errors due to photon loss

The photon loss is attributed to two physical processes: the spontaneous decay with rate γ for the optically excited state $|e\rangle$ (Fig. 2b), and the cavity loss with rate κ during the QND interaction. For single photon approach, the interaction time is $\tau = \pi/2\chi$ and the effective spontaneous decay rate is suppressed to $\frac{g^2}{\Delta^2}\gamma$ by having large detuning $\Delta \gg g$ for each selected spin (Fig. 2b). Under the assumption that the selected spins decay independently, the total probability for photon loss is

$$\kappa\tau + N\frac{g^2}{\Delta^2}\gamma\tau \geq 2\pi\sqrt{N/P} \equiv P_{\text{loss}},$$

where we define the Purcell factor $P \equiv g^2/\kappa\gamma$ [29, 30]. And the minimum probability can be achieved by choosing optimal detuning $\Delta = g\sqrt{N\gamma/\kappa}$.

For geometric phase gate approach, we can choose $|\alpha|^2 = |\beta|^2 = \pi/2$ so that the total probability for photon loss is $P_{\text{loss}} \approx |\alpha|^2 \left(\kappa\tau + N\frac{g^2}{\Delta^2}\gamma\tau \right)$ with $\tau \approx \pi\Delta/g^2$. Similar to single photon approach, the probability P_{loss} can be significantly reduced by having a large Purcell factor $P > N$. For coherent states, we cannot identify photon loss events unambiguously, but we can still characterize the errors associated with the photon loss.

The deviation of the QND interaction

The dominant deviation of the QND interaction is from the fluctuations of the coupling strength between the cavity mode

and selected spins, described by the following perturbation

$$\delta H = \chi a^\dagger a \sum_{j \in C} \delta_j \sigma_j^z,$$

where δ_j is the relative deviation for the j th spin. In the presence of cavity excitation, the implementation of the gate $U_j = \exp(i\theta\sigma_j^z)$ on the j th spin could lead to the gate $\tilde{U}_j = \exp[i(1 + \delta_j)\theta\sigma_j^z]$. We define the error by the operator norm $\epsilon_j \equiv \|\tilde{U}_j - U_j\| \approx \theta|\delta_j|$ [48]. Thus we have the error for the QND interaction, $P_{\text{QND}} \equiv \|\prod_{j \in C} \tilde{U}_j - \prod_{j \in C} U_j\| \leq \sum_j \epsilon_j$.

This kind of error due to inhomogeneity can be compensated in two ways. First one could add an optical potential to the system which is shaped to equalize the couplings δ_j for all the spins along the configuration path C . A second option is to use composite pulse sequences on the system in which case it has been shown that the error can be reduced to $O(|\delta_j|^k)$ for $\forall j$ using $O(k^3)$ pulses [32]. Therefore, $P_{\text{QND}} \sim N_C \theta |\delta|^k$ is effectively suppressed.

Summary

Combining all the decoherence mechanisms, the error probability for the swap in- swap-out process with memory storage time t is

$$p_{\text{topo-mem}} = (\delta h/J)^N qt + 4\lambda\sqrt{N/P} + N\epsilon,$$

with the pre-factor $\lambda = 2\pi$ (and $4\pi^2$) for the single photon (and geometric phase gate) approach. Compared with the storage error without topological encoding $p_{\text{ref-mem}} = q \times t$, for storage time $t > \frac{4\lambda\sqrt{N/P} + N\epsilon}{q} \approx \frac{4\lambda\sqrt{N/P}}{q}$, our topological memory outperforms storage in a single quantum system.

We remark that for single photon approach, photon loss induces leakage errors that can be detected without compromising the state stored in the topological memory. Such detected errors can be overcome by repetition, which is applicable to probabilistic operations such as entanglement generations in quantum repeater [19] and distributed quantum computer [36]. Detected errors can have a very high tolerable threshold for deterministic quantum computation schemes [49].

Fringe contrast of the interferometer in the presence of excitations

We refer to anyons left from the initialization as *quenched anyons*, which can result in measurable effects to the phase measurement associated with braiding [equation (5)]. To be specific, we will consider the planar code, and assume that the probability to have one pair of initial anyons is p while neglecting the case with multiple pairs of anyons. If the anyons are immobile (e.g., the braiding operation is much faster than anyonic propagation), the contrast of the phase measurement only depends the probability that the loop $l_1 \cup l_3$ (or $l'_2 \cup l'_4$)

(see Fig. 4a) encloses an odd number of initial x-particles (or z-particles). An extra phase $e^{i\theta} = -1$ will be accumulated from each loop satisfying this condition. Suppose the loop $l_1 \cup l_3$ (or $l'_2 \cup l'_4$) encloses m faces (or m' vertices). If one pair of initial x-particles is uniformly distributed among $N^2 \times (N^2 - 1)/2$ possible configurations, the probability for accumulating an extra phase is $q_m \equiv \frac{2m(N^2 - m)}{N^2(N^2 - 1)}$ for the loop $l_1 \cup l_3$. The probability reaches a maximum value $\approx 1/2$ for $m \approx N^2/2$; meanwhile it vanishes for $m = 0$ or N^2 , which is achieved by $l_1 = l_3$. Therefore, the contrast for the fringes of $\langle \sigma_\phi \rangle$ v.s. ϕ will be reduced to $1 - p \times (q_m + q_{m'})$.

If the anyons are highly diffusive (e.g., random anyonic propagation is very fast compared to the intervals between the control operations), we should avoid adding any anyons by applying string operators that act within the ground subspace of the topological memory. As shown in Fig. 4c, we use generators of the encoded qubits associated with strings $\{l_{Z1}, l'_{X2}, l_{Z3}, l'_{X4}\}$ to implement the braiding operation. However, any quenched anyons (if present) will quickly diffuse over the entire torus and completely wash away the fringe of $\langle \sigma_\phi \rangle$. Therefore, the remaining contrast with highly diffusive anyons is $1 - p$. Note that imperfect string operators may also reduce the contrast, since they may introduce unwanted anyons to the topological memory with probability approximately proportional to the length of the string.

Extension to \mathbb{Z}_d gauge theories

This interferometric technique can be extended to measure abelian anyonic statistics for any \mathbb{Z}_d gauge theory by introducing the spin lattice Hamiltonian with d levels for each spin [50]. One can still use a probe qubit to measure the statistical phase via controlled-string operations. The mutual statistical phase between a charge $a \in \mathbb{Z}_d$ and flux $b \in \mathbb{Z}_d$ associated with the braiding operation is $\tilde{Z}_{C_Z}^{-a} \tilde{X}_{C_X}^{-b} \tilde{Z}_{C_Z}^a \tilde{X}_{C_X}^b = e^{i2\pi ab/d}$. Here the string operator $\tilde{Z}_{C_Z}^a (\tilde{X}_{C_X}^b)$ is a product of $Z^a (X^b)$ operators of all the spins on the string $C_Z (C_X)$, where Z and X are elements of the generalized Pauli group. The operator Z can be implemented by phasing pairs of spin states at a time using the protocols in the main text for the appropriate duration at each stage. Equivalently, one can choose field polarizations and detunings so that only one of the d levels is strongly coupled to the cavity, then evolve that state for the appropriate time, and swap other states in, evolve, and swap out again. A total of $d - 1$ global gates suffice to simulate $\tilde{Z}_{C_Z}^a$. The same follows for the $\tilde{X}_{C_X}^b$ operators, but one must perform a parallel Fourier transform operator $F = \prod_{j \in C_X} f_j$ first on all the spins in the configuration, then implement $\tilde{Z}_{C_X}^b$ then apply F^{-1} .

University Press, Oxford, (2004).

- [2] Einarsson, T. Fractional statistics on a torus. *Phys. Rev. Lett.* **64**, 1995 (1990).
- [3] Das Sarma, S., Freedman, M., Nayak, C., Simon, S. H., and Stern, A. Non-abelian anyons and topological quantum computation. *e-print arXiv: 0707.1889* (2007).
- [4] Camino, F. E., Zhou, W., and Goldman, V. J. Realization of a Laughlin quasiparticle interferometer: Observation of fractional statistics. *Phys. Rev. B* **72**, 075342–8 (2005).
- [5] Rosenow, B. and Halperin, B. I. Influence of interactions on flux and back-gate period of quantum hall interferometers. *Phys. Rev. Lett.* **98**, 106801–4 (2007).
- [6] Duan, L. M., Demler, E., and Lukin, M. D. Controlling spin-exchange interactions of ultracold atoms in optical lattices. *Phys. Rev. Lett.* **91**, 090402 (2003).
- [7] Micheli, A., Brennen, G. K., and Zoller, P. A toolbox for lattice-spin models with polar molecules. *Nat. Phys.* **2**, 341–347 (2006).
- [8] Brennen, G. K. and Pachos, J. K. Why should anyone care about computing with anyons? *Proc. R. Soc. London, A* **10.1098/rspa.2007.0026** (2007).
- [9] Pachos, J. K. The wavefunction of an anyon. *Ann. Phys.* **322**, 1254–1264 (2007).
- [10] Zhang, C. W., Scarola, V. W., Tewari, S., and Das Sarma, S. Anyonic braiding in optical lattices. *e-print arXiv: quant-ph/0609101* (2006).
- [11] Mabuchi, H. and Doherty, A. C. Cavity quantum electrodynamics: Coherence in context. *Science* **298**, 1372–1377 (2002).
- [12] Gupta, S., Moore, K. L., Murch, K. W., and Stamper-Kurn, D. M. Cavity nonlinear optics at low photon numbers from collective atomic motion. *e-print arXiv: 0706.1052* (2007).
- [13] Colombe, Y., Steinmetz, T., Dubois, G., Linke, F., Hunger, D., and Reichel, J. Strong atom-field coupling for Bose-Einstein condensates in an optical cavity on a chip. *e-print arXiv: 0706.1390* (2007).
- [14] Brennecke, F., Donner, T., Ritter, S., Bourdel, T., Kohl, M., and Esslinger, T. Cavity qed with a Bose-Einstein condensate. *e-print arXiv: 0706.3411* (2007).
- [15] Cirac, J. I. and Zoller, P. Quantum computations with cold trapped ions. *Phys. Rev. Lett.* **74**, 4091 (1995).
- [16] Lu, C.-Y., Gao, W.-B., Guhne, O., Zhou, X.-Q., and Chen, Z.-B. Demonstration of fractional statistics of anyons in the Kitaev lattice-spin model. *e-print arXiv: 0710.0278* (2007).
- [17] Pachos, J. K., Wieczorek, W., Schmid, C., Kiesel, N., Pohlner, R., and Weinfurter, H. Revealing anyonic statistics with multiphoton entanglement. *e-print arXiv: 0710.0895* (2007).
- [18] Han, Y. J., Raussendorf, R., and Duan, L. M. Scheme for demonstration of fractional statistics of anyons in an exactly solvable model. *Phys. Rev. Lett.* **98**, 150404–4 (2007).
- [19] Briegel, H. J., Dur, W., Cirac, J. I., and Zoller, P. Quantum repeater: The role of imperfect local operations in quantum communication. *Phys. Rev. Lett.* **81**, 5932 (1998).
- [20] Jiang, L., Taylor, J. M., Khaneja, N., and Lukin, M. D. Optimal approach to quantum communication algorithms using dynamics programming. *Proc. Natl. Acad. Sci. U. S. A.* **104**, 17291 (2007).
- [21] Kitaev, A. Y. Fault-tolerant quantum computation by anyons. *Ann. Phys.* **303**, 2–30 (2003).
- [22] Dennis, E., Kitaev, A., Landahl, A., and Preskill, J. Topological quantum memory. *J. Math. Phys.* **43**, 4452–4505 (2002).
- [23] Kitaev, A. Anyons in an exactly solved model and beyond. *Ann. Phys.* **321**, 2–111 (2006).
- [24] Walls, D. F. and Milburn, G. J. *Quantum optics*. Springer, Berlin ; New York, (1994).

[1] Wen, X.-G. *Quantum field theory of many-body systems : from the origin of sound to an origin of light and electrons*. Oxford

- [25] Scully, M. O. and Zubairy, M. S. *Quantum optics*. Cambridge University Press, Cambridge ; New York, (1997).
- [26] Cho, J. Addressing individual atoms in optical lattices with standing-wave driving fields. *Phys. Rev. Lett.* **99**, 020502–4 (2007).
- [27] Gorshkov, A., Jiang, L., Greiner, M., Zoller, P., and Lukin, M. D. Coherent quantum optical control with sub-wavelength resolution. *e-print arXiv: 0706.3879* (2007).
- [28] Wang, X. and Zanardi, P. Simulation of many-body interactions by conditional geometric phases. *Phys. Rev. A* **65**, 032327 (2002).
- [29] Purcell, E. M. Spontaneous emission probabilities at radio frequencies. *Phys. Rev.* **69**, 681–681 (1946).
- [30] Michler, P., Kiraz, A., Becher, C., Schoenfeld, W. V., Petroff, P. M., Zhang, L. D., Hu, E., and Imamoglu, A. A quantum dot single-photon turnstile device. *Science* **290**, 2282–2285 (2000).
- [31] Vandersypen, L. M. K. and Chuang, I. L. Nmr techniques for quantum control and computation. *Rev. Mod. Phys.* **76**, 1037–1069 (2004).
- [32] Brown, K. R., Harrow, A. W., and Chuang, I. L. Arbitrarily accurate composite pulse sequences. *Phys. Rev. A* **70**, 052318–4 (2004).
- [33] Duan, L. M., Blinov, B. B., Moehring, D. L., and Monroe, C. Scalable trapped ion quantum computation with a probabilistic ion-photon mapping. *Quantum Inf. Comput.* **4**, 165 (2004).
- [34] Lim, Y. L., Barrett, S. D., Beige, A., Kok, P., and Kwek, L. C. Repeat-until-success quantum computing using stationary and flying qubits. *Phys. Rev. A* **73**, 012304 (2006).
- [35] Benjamin, S. C., Browne, D. E., Fitzsimons, J., and Morton, J. J. L. Brokered graph-state quantum computation. *New J. Phys.* **8**, 141 (2006).
- [36] Jiang, L., Taylor, J. M., Sorensen, A., and Lukin, M. D. Scalable quantum networks based on few-qubit registers. *e-print arXiv: quant-ph/0703029* (2007).
- [37] Jiang, L., Taylor, J. M., Sorensen, A., and Lukin, M. D. Distributed quantum computation based-on small quantum registers. *e-print arXiv: 0709.4539* (2007).
- [38] Arovas, D., Schrieffer, J. R., and Wilczek, F. Fractional statistics and the quantum hall effect. *Phys. Rev. Lett.* **53**, 722 (1984).
- [39] Freedman, M., Nayak, C., and Shtengel, K. Extended hubbard model with ring exchange: A route to a non-abelian topological phase. *Phys. Rev. Lett.* **94**, 066401–4 (2005).
- [40] Doucot, B., Feigel'man, M. V., Ioffe, L. B., and Ioselevich, A. S. Protected qubits and chern-simons theories in josephson junction arrays. *Phys. Rev. B* **71**, 024505–18 (2005).
- [41] Nielsen, M. A. and Chuang, I. *Quantum computation and quantum information*. Cambridge University Press, Cambridge, U.K. ; New York, (2000).
- [42] Ramsey, N. F. Experiments with separated oscillatory fields and hydrogen masers. *Rev. Mod. Phys.* **62**, 541 (1990).
- [43] Bacon, D. Operator quantum error-correcting subsystems for self-correcting quantum memories. *Phys. Rev. A* **73**, 012340–13 (2006).
- [44] Milman, P., Mainault, W., Guibal, S., Guidoni, L., Doucot, B., Ioffe, L., and Coudreau, T. Topologically decoherence-protected qubits with trapped ions. *Phys. Rev. Lett.* **99**, 020503–4 (2007).
- [45] Levin, M. A. and Wen, X. G. String-net condensation: A physical mechanism for topological phases. *Phys. Rev. B* **71**, 045110 (2005).
- [46] Hastings, M. B. and Wen, X.-G. Quasiadiabatic continuation of quantum states: The stability of topological ground-state degeneracy and emergent gauge invariance. *Phys. Rev. B* **72**, 045141–14 (2005).
- [47] Aguado, M., Brennen, G. K., Cirac, J. I., and Verstraete, F. (In preparation).
- [48] Bhatia, R. *Matrix analysis*. Springer, New York, (1997).
- [49] Knill, E. Scalable quantum computing in the presence of large detected-error rates. *Phys. Rev. A* **71**, 042322–7 (2005).
- [50] Bullock, S. S. and Brennen, G. K. Qudit surface codes and gauge theory with finite cyclic groups. *Journal of Physics a-Mathematical and Theoretical* **40**, 3481–3505 (2007).

ACKNOWLEDGEMENTS

We gratefully acknowledge conversations with H. P. Buchler, L. Ioffe, and A. M. Rey. Work at Harvard is supported by NSF, ARO-MURI, CUA, and the Packard Foundation. Work at Innsbruck is supported by the Austrian Science Foundation, the EU under grants OLAQUI, SCALA, and the Institute for Quantum Information.

COMPETING FINANCIAL INTERESTS

The authors declare that they have no competing financial interests.

Supplementary Online Materials

NOISE MODEL FOR TORIC-CODE HAMILTONIAN

The toric-code Hamiltonian for spins on the edges of $N \times N$ square lattice

$$H_{\text{topo}} = -J \sum_s A_s - J \sum_p B_p, \quad (8)$$

is a sum of stabilizer operators $A_s = \prod_{j \in \text{star}(s)} \sigma_j^x$ and $B_p = \prod_{j \in \text{boundary}(p)} \sigma_j^z$ associated with the site (vertex) s and the plaquette (face) p , respectively. And the coupling strength J determines the energy gap between the ground and excited states $\Delta \sim J$, which is also the energy associated with the quasi-particle excitations. There are two types of quasi-particles: (1) z -particles that live on the vertices of the lattice and (2) x -particles that live on the plaquette. The quasi-particles do not change from one type to the other type, but there is a non-trivial topological phase associated with braiding of two quasi-particles of different type. We generate and move these quasi-particles by applying string operators, meanwhile during the interval between the string operators the quasi-particles will evolve under the toric-code Hamiltonian and various local perturbations from the environment. In the absence of perturbations from the environment, the quasi-particles are immobile. However, the mobility of quasi-particles changes when we include local perturbations, because the excited states with quasi-particles are highly degenerate and any small perturbation to the Hamiltonian can change both the energy spectrum and the eigenwavefunctions.

Perturbation Hamiltonian

In this section, we will consider a simple model that will induce diffusion of quasi-particles of the toric-code Hamiltonian. We will consider the case that the perturbation is small compared to the energy gap Δ , so that the number of quasi-particles is still conserved. However, we will show that such small perturbation can lead to non-trivial dynamics in the manifold with fixed number of quasi-particles. The perturbation is described by the Hamiltonian

$$H_{\text{pert}} = \sum_{e \in \text{All spins}} h_e \sigma_e^x \quad (9)$$

where e is the label for spins that we sum over. The time dependent coefficient h_e is the local field associated with spin e .

We can also write the perturbation Hamiltonian by summing over the plaquettes and their surrounding edges:

$$H_{\text{pert}} = \frac{1}{2} \sum_p \sum_{\eta \in \mathcal{N}} h_{p,\eta} \sigma_{p,\eta}^x, \quad (10)$$

where p is the label for the plaquette, η is the label for the surrounding edges, $\mathcal{N} = \{(0,1), (0,-1), (1,0), (-1,0)\}$ is the set that includes four edges around the plaquette as illustrated in Fig. 6a. The combination of (p, η) label the η -edge of plaquette p . We use $h_{p,\eta}$ and $\sigma_{p,\eta}^x$ to represent the local fluctuating field and the spin operator for edge (p, η) , respectively. Since each edge is shared by two neighboring plaquettes, both (p, η) and $(p + \eta, -\eta)$ represent the same edge. By definition, we have $h_{p,\eta} \equiv h_{p+\eta, -\eta}$ and $\sigma_{p,\eta}^x \equiv \sigma_{p+\eta, -\eta}^x$. The prefactor $1/2$ in Eq. (9) accounts for the double counting of edges.

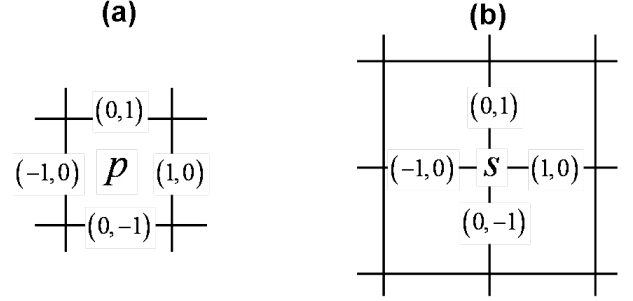


FIG. 6: Relative position of edges with respect to (a) plaquette and (b) site.

Effects from Perturbation

We now consider the effects from the perturbation Hamiltonian H_{pert} , under the assumption that the number of quasi-particles is conserved. This assumption can be justified as long as the local fluctuating field has a small amplitude and low-frequency noise spectrum, compared with the energy gap from the topological Hamiltonian. For ground states of the toric-code Hamiltonian, there are no quasi-particle excitations. And the perturbation Hamiltonian can only induce *virtual* excitations of quasi-particles. Thus the leading non-trivial effect within the ground-state manifold is the N th order perturbative process, associated with hopping of virtual quasi-particles along a minimal non-contractible loop of length N . Such N th order process is suppressed by a factor $(|h|/\Delta)^N$ which decreases exponentially with respect to the system size. As expected, the ground states of the topological Hamiltonian should be robust against these local perturbations.

The perturbation Hamiltonian acts very differently on the excited states. It can induce x -particles to hop to the neighboring plaquettes, while having no influence to z -particles. We may define the creation operator of the x -particle at plaquette p as b_p^\dagger , which changes the stabilizer B_p from $+1$ to -1 . Similarly, the annihilation operator b_p changes B_p from -1 to $+1$. By definition, $(b_p^\dagger)^2 = (b_p)^2 = 0$. Applying σ^x to one of the edge of the plaquette will flip the sign of the stabilizer B_p , represented by $b_p + b_p^\dagger$. Since each edge is shared by two neighboring plaquettes, $\sigma_{p,\eta}^x$ will flip both stabilizers B_p and

$B_{p+\eta,-\eta}$, which can be expressed as

$$\sigma_{p,\eta}^x \rightarrow (b_p + b_p^\dagger) (b_{p+\eta} + b_{p+\eta}^\dagger). \quad (11)$$

By conservation of quasi-particles, we can simplify the mapping:

$$\sigma_{p,\eta}^x \rightarrow b_p b_{p+\eta}^\dagger + b_p^\dagger b_{p+\eta}. \quad (12)$$

Therefore, within the manifold of fixed quasi-particles, the perturbation Hamiltonian can be reduced to

$$H'_{pert} = \frac{1}{2} \sum_p \sum_{\eta \in \mathcal{A}} h_{p,\eta} (b_p b_{p+\eta}^\dagger + b_p^\dagger b_{p+\eta}), \quad (13)$$

where the local field $h_{p,\eta}$ can also be interpreted as the tunneling rate of quasi-particles from p to $p + \eta$, or from $p + \eta$ to p .

We now use H'_{pert} to study the dynamics of quasi-particles. Suppose at time $t = 0$ we create an x-particle at plaquette p

$$|\varphi_0\rangle = b_p^\dagger |vac\rangle. \quad (14)$$

And at a later time τ the state becomes

$$\begin{aligned} |\varphi_\tau\rangle &= \exp[-iH'_{pert}\tau] b_p^\dagger |vac\rangle \\ &= \left[1 - \sum_{\eta} (h_{p,\eta}\tau)^2 \right] b_p^\dagger |vac\rangle + \sum_{\eta} (h_{p,\eta}\tau) b_{p+\eta}^\dagger |vac\rangle \\ &\quad + O(h^3\tau^3), \end{aligned} \quad (15)$$

where in the second equality we assume that $h_{p,\eta}$ is *time-independent* and expand only to the second order of $h_{p,\eta}\tau$. The overlap between the initial and final states is

$$\langle\varphi_0|\varphi_\tau\rangle \approx 1 - \sum_{\eta} (h_{p,\eta}\tau)^2 \approx \exp\left[-\sum_{\eta} h_{p,\eta}^2 \tau^2\right]. \quad (16)$$

Therefore, for time-independent perturbation and relatively short waiting time (i.e., $\tau \ll h_{p,\eta}^{-1}$), the probability for a quasi-particle to remain at the same position decreases *quadratically* with time.

Generally, the local field $h_{p,\eta}$ will depend on time and we should replace $h_{p,\eta}\tau$ by $\int_0^\tau h_{p,\eta}(t') dt'$ in the equations above. In particular, the local field $h_{p,\eta}(t')$ can be a stochastic random variable. In the next section, we will study the dynamics associated with stochastic noise fields $\{h_{p,\eta}\}$.

Time-dependent Perturbation

We now consider the local stochastic noise fields characterized by the auto-correlation function

$$f(t) \equiv \overline{h_{p,\eta}(t') h_{p,\eta}(t'+t)}, \quad (17)$$

where we assume that $h_{p,\eta}$ is steady and the auto-correlation only depends on the time difference between the two sampling points. For simplicity, we will also assume independent local noise for different spins; that is the correlation function $\overline{h_{p,\eta}(0) h_{p',\eta'}(t)}$ vanishes unless (p, η) and (p', η') represent the same spin. We can characterize the noise by using the power spectrum density, which is the Fourier transform of the auto-correlation function:

$$\tilde{f}(\omega) \equiv \frac{1}{2\pi} \int_{-\infty}^{\infty} f(t) e^{-i\omega t} dt. \quad (18)$$

For example, the Gaussian correlation function

$$f(t) = \xi_h^2 \exp[-t^2/\tau_c^2] \quad (19)$$

has power spectrum density

$$\tilde{f}(\omega) = \frac{\xi_h^2}{\sqrt{\pi}\omega_c} \exp[-\omega^2/\omega_c^2], \quad (20)$$

where the typical amplitude of the stochastic field is ξ_h , the correlation time is τ_c , and the cut-off frequency is $\omega_c = 2\tau_c^{-1}$. The power spectrum density vanishes for high frequency $\omega \gg \omega_c$.

We can estimate the probability for a quasi-particle to remain in the same position, in the presence of local stochastic noise,

$$\begin{aligned} p_\tau &= \overline{|\langle\varphi_0|\varphi_\tau\rangle|^2} \\ &\approx 1 - 2 \sum_{\eta \in \mathcal{A}} \overline{\left(\int_0^\tau h_{p,\eta}(t') dt' \right)^2}. \end{aligned} \quad (21)$$

We first evaluate the square average of the integral for the fluctuation field

$$\begin{aligned} &\overline{\left(\int_0^\tau h_{p,\eta}(t') dt' \right)^2} \\ &= \int_0^\tau \int_0^\tau \overline{h_{p,\eta}(t') h_{p,\eta}(t'')} dt' dt'' \\ &= \int_{-\infty}^{\infty} \frac{\sin^2(\omega\tau/2)}{(\omega\tau/2)^2} \tilde{f}(\omega) d\omega \\ &\approx 2\pi \tilde{f}(\omega=0) \tau, \end{aligned} \quad (22)$$

where the last step assumes that we are interested in a time scale much longer than the noise correlation time: $\tau \gg \tau_c$. Plugging Eq. (22) into Eq. (21), we get the probability

$$p_\tau \approx \exp[-2z\Gamma\tau], \quad (23)$$

where $z = |\mathcal{A}| = 4$ is the coordination number of the square lattice, and $\Gamma = 2\pi\tilde{f}(\omega=0)$ is the diffusion rate to each neighboring position. For Gaussian correlation [Eq. (19)], the diffusion rate is

$$\Gamma = 2\sqrt{\pi}\xi_h^2/\omega_c. \quad (24)$$

Fringe Contrast for Interference Experiment

We now consider how diffusion of quasi-particles affect the fringe contrast of the anyonic interferometry. The signal of the anyonic interferometry is attributed to the interference from path-ways with different braiding of anyonic quasi-particles, which is achieved by using controlled-string operations. During the intervals between the controlled-string operations, the quasi-particles excited by the controlled-string operations will diffuse, and the final state of the topological memory will have components orthogonal to the initial state. Since the orthogonal components do not contribute to the fringes, the contrast will be reduced.

The anyonic interferometry is analogous to the Ramsey experiment in the following aspects. For both cases, we start with a superposition state $|0\rangle + |1\rangle$ for some two level system. Then, we let the system evolve, and meanwhile it is also interacting with the environment (e.g., cavity mode and selected spins, or external magnetic field). Finally, we projectively measure the system in some basis $|0\rangle \pm e^{\pm i\phi} |1\rangle$. The reduction of the measurement signal is attributed to various decoherence processes. For Ramsey experiment, the dominant decoherence is induced by fluctuations of the external magnetic field and it is characterized by the dephasing time T_2^* . For anyonic interferometry, we can define a similar dephasing time

$$T_2^* = \frac{1}{z\Gamma}. \quad (25)$$

And the fringe contrast is equal to the averaged overlap function, which can be expressed as

$$|\langle \Phi_0 | \Phi_\tau \rangle| \approx \exp[-\tau/T_2^*]. \quad (26)$$

For stochastic noise with Gaussian correlation [Eq. (19)], we have $T_2^* = \omega_c / (2z\sqrt{\pi}\xi_h^2)$.

Spin Echo Techniques

Similar to NMR systems, we can also use spin-echo techniques to further suppress the stochastic noise. The essence of spin-echo is to apply an effective time-reversal operation in the mid of the evolution so that the noises from the two intervals cancel each other. For anyonic interferometry, the effective time-reversal operation for the perturbation H_{pert} is

$$U_\pi^z \equiv \prod_{e \in \text{All spins}} \sigma_e^z. \quad (27)$$

This is because $\{H_{pert}, U_\pi^z\} = 0$ and $[H_{topo}, U_\pi^z] = 0$. For example, at time $t = 0$ we create an x-particle at plaquette p

$$|\Phi_0\rangle = b_p^\dagger |vac\rangle, \quad (28)$$

We apply U_π^z operations at time $\tau/2$ and τ . The final state will be

$$\begin{aligned} & |\Phi_\tau^{echo}\rangle \\ &= U_\pi^z e^{-i \int_{\tau/2}^\tau H'_{pert}(t') dt'} U_\pi^z e^{-i \int_0^{\tau/2} H'_{pert}(t') dt'} b_p^\dagger |vac\rangle \\ &= e^{-i \int_0^{\tau/2} [H'_{pert}(t') - H'_{pert}(\tau/2+t')] dt'} b_p^\dagger |vac\rangle. \end{aligned} \quad (29)$$

For stochastic noise with Gaussian correlation [Eq. (19)], the averaged overlap function now becomes

$$|\langle \Phi_0 | \Phi_\tau^{echo} \rangle| \approx \exp\left[-(\tau/T_2)^4\right] \quad (30)$$

where $T_2 \sim \sqrt{\tau_c/\xi_h}$. Since $T_2 \sim T_2^* \times (\tau_c \xi_h)^{3/2}$, for $\tau_c \xi_h > 1$ we can extend the coherence time by using echo-techniques.

Furthermore, we may introduce n pairs of time-reversal operations within the time interval τ (e.g., the pulse sequence $\underbrace{U_\pi^z \dots U_\pi^z}_{\text{Repeat } n \text{ times}} \dots U_\pi^z$). And the time dependence of the constrast becomes

$$\exp\left[-\frac{1}{n^3} \left(\frac{\tau}{T_2}\right)^4\right].$$

The contrast reduction is further slow down by a factor of $n^{3/4}$ and this is illustrated in Fig. 5 of the paper.

General Perturbation Hamiltonian

We now generalize the perturbation Hamiltonian by including stochastic fields along z direction

$$H_{pert,gen} = \sum_{e \in \text{All spins}} h_e^x \sigma_e^x + h_e^y \sigma_e^y + h_e^z \sigma_e^z. \quad (31)$$

We introduce the creation (and annihilation) operators a_s^\dagger (and a_s) for z -particles at site s . Suppose the edge e connects two sites s and $s+\zeta$ and it is also shared by two plaquettes p and $p+\eta$ (see Fig. 6). Within the manifold of fixed number of quasi-particles, we have the following mapping:

$$\sigma_e^x \rightarrow b_p b_{p+\eta}^\dagger + b_p^\dagger b_{p+\eta} \quad (32)$$

$$\sigma_e^z \rightarrow a_s a_{s+\zeta}^\dagger + a_s^\dagger a_{s+\zeta} \quad (33)$$

Thus, the σ_e^x term leads to hopping of x -particles, while the σ_e^z term leads to hopping of z -particles. The σ_e^y term leads to hopping of *dyonic particles* (paired x -particle and z -particle sharing the same edge, e.g., $a_s^\dagger b_p^\dagger$)

$$\sigma_e^y = i[\sigma_e^x, \sigma_e^z] \rightarrow i[b_p b_{p+\eta}^\dagger + b_p^\dagger b_{p+\eta}, a_s a_{s+\zeta}^\dagger + a_s^\dagger a_{s+\zeta}]. \quad (34)$$

And the effective operator for σ_e^y is still Hermitian. Note that σ_e^y consists of terms like $i(b_p b_{p+\eta}^\dagger a_s a_{s+\zeta}^\dagger - a_s a_{s+\zeta}^\dagger b_p b_{p+\eta}^\dagger)$,

and the minus sign for terms with different order is consistent with the phase associated with the braiding of anyons.

The generalized effective Hamiltonian becomes

$$\begin{aligned}
H'_{\text{pert,gen}} &= \frac{1}{2} \sum_p \sum_{\eta \in \mathcal{N}} h_{p,\eta}^x \left(b_p b_{p+\eta}^\dagger + b_p^\dagger b_{p+\eta} \right) \\
&+ \frac{1}{2} \sum_s \sum_{\zeta \in \mathcal{N}} h_{s,\zeta}^z \left(a_s a_{s+\zeta}^\dagger + a_s^\dagger a_{s+\zeta} \right) \\
&+ \frac{1}{4} \sum_{e \in \text{All spins}} i h_e^y \left[b_p b_{p+\eta}^\dagger + b_p^\dagger b_{p+\eta}, a_s a_{s+\zeta}^\dagger + a_s^\dagger a_{s+\zeta} \right].
\end{aligned} \quad (35)$$

where the first term induces hopping of x-particles and the second term for z-particles. These two terms commute with each other, except for the situation when (p, η) and (s, ζ) represents the same edge. The third term induces hopping of dyonic particles. If we are studying diffusion property of quasi-particles that are far apart, there is essentially no dyonic particles and we may safely neglect the effect from the third term. Therefore, as long as the diffusion does not induce braiding of quasi-particles, we can safely treat the diffusion for x-particles and z-particles as independent processes.

We may also introduce the effective time-reversal operation $U_\pi^x \equiv \prod_{e \in \text{All spins}} \sigma_e^x$ for perturbations of $\sum_{e \in \text{All spins}} h_e^z \sigma_e^z$, since they anti-commute $\{h_e^z \sigma_e^z, U_\pi^x\} = 0$. We can combine U_π^z and U_π^x in a nested fashion to suppress the diffusion of **both** x-particles and z-particles:

$$U_\pi^z \left(\dots U_\pi^x \dots U_\pi^x \dots \right) U_\pi^z \left(U_\pi^x \dots U_\pi^x \dots \right).$$

which can be further simplified as:

$$U_\pi^z \dots U_\pi^x \dots U_\pi^z \dots U_\pi^x \dots \quad (36)$$

Note that since time reversal operations U_π^x and U_π^z also anti-commute with $\sum_{e \in \text{All spins}} h_e^z \sigma_e^z$, the nest combination of the two also suppress the diffusion of dyonic particles. Therefore, we are able to suppress diffusion induced by the general perturbation Hamiltonian of Eq. (31) to higher order.

Time Reversal Operations for Surface-Code Hamiltonian with Boundaries

We now consider the effective time-reversal operations for the surface-code Hamiltonian with boundaries. For the planar code on a square lattice (see Fig. 1a of the paper), at the left and right are "rough edges" where the stabilizer operator B_p is a product of three σ^x spin operators associated with each boundary plaquette, while at the top and bottom are "smooth edges" where the stabilizer operator A_s is a product of three σ^z spin operators associated with each boundary site. In contrast to the stabilizers associated with interior sites and plaquettes, these boundary stabilizers anti-commute with the previous echo unitary U_π^x or U_π^z . Thus, we have to modify the echo unitaries, so that they commute with all stabilizers.

Let us first consider the modification of U_π^z . We refer to the boundary protruding edges in even rows as "even rough edges," and those in odd row as "odd rough edges." We define $U_\pi^{x,e} \equiv \prod_{\substack{e \in \text{All spins} \\ e \notin \text{Odd rough edges}}} \sigma_e^x$ and $U_\pi^{x,o} \equiv \prod_{\substack{e \in \text{All spins} \\ e \notin \text{Even rough edges}}} \sigma_e^x$, so that $U_\pi^{x,e}$ and $U_\pi^{x,o}$ act on even and odd boundary edges, respectively. After this modification, both $U_\pi^{x,e}$ and $U_\pi^{x,o}$ commute with all stabilizers, especially B_p at the left and right "rough edges." Similarly, we label "even/odd smooth edges" associated the columns for the top and bottom "smooth edges," and modify U_π^x into $U_\pi^{z,e} \equiv \prod_{\substack{e \in \text{All spins} \\ e \notin \text{Odd smooth edges}}} \sigma_e^z$ and $U_\pi^{z,o} \equiv \prod_{\substack{e \in \text{All spins} \\ e \notin \text{Even smooth edges}}} \sigma_e^z$, which commute with all stabilizers.

We introduce the sub-sequence

$$W^{\alpha,\beta}(\tau) \equiv U_\pi^{z,\alpha} \dots U_\pi^{x,\beta} \dots U_\pi^{z,\alpha} \dots U_\pi^{x,\beta} \dots,$$

for $\alpha, \beta = e$ or o . And finally the full echo sequence to suppress anyonic diffusion for the surface-code Hamiltonian with boundaries is

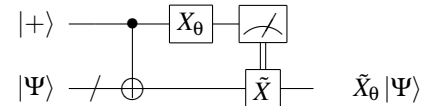
$$W^{e,e}(\tau/4) W^{e,o}(\tau/4) W^{o,e}(\tau/4) W^{o,o}(\tau/4). \quad (37)$$

Summary

In summary, we have analyzed a simple noise model on top of the toric-code Hamiltonian. We have found that this noise model can explain diffusion of quasi-particles. For anyonic interferometry, the effect of quasi-particle diffusion is analogous to the dephasing of the Ramsey experiment. Based on this analogy, we have proposed a scheme to extend the spin-echo technique to the topological memory, which will further suppress the diffusion of quasi-particles.

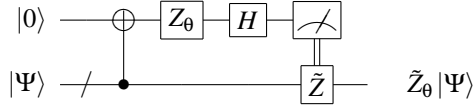
UNIVERSAL ROTATIONS ON THE TOPOLOGICAL MEMORY

We can achieve universal rotations of the encoded qubit stored in the topological memory. For example, an arbitrary x-rotation $\tilde{X}_\theta = e^{i\theta \tilde{X}}$ on the topological memory can be achieved via the gate teleportation circuit



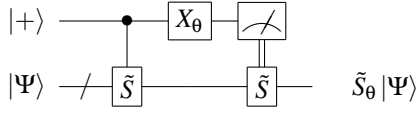
This circuit represents the following procedure: (1) use controlled-string operation $\Lambda[\tilde{X}]$ to entangle the probe qubit (upper line) and the memory (lower line with a slash), (2) projectively measure the probe qubit in a rotated basis, and (3) perform an encoded Pauli X gate over the topological memory conditioned on the measurement outcome. Similarly, we

can also implement arbitrary z-rotation $\tilde{Z}_\theta = e^{i\theta\tilde{Z}}$ on the topological memory via the gate teleportation circuit



Since any rotation can be decomposed into a sequence of x- and z-rotations, the above two circuits suffice for universal rotations.

The gate teleportation can be generalized to implement arbitrary unitaries generated by string operators. For string operator \tilde{S} , the unitary operation $\tilde{S}_\theta = e^{i\theta\tilde{S}}$ can be achieved via the gate teleportation circuit



For the geometric phase gate scheme, we can actually implement rotations of the encoded qubit without the probe qubit, e.g., x-rotation of the encoded qubit can be decomposed as $e^{i\theta\tilde{X}} = D(-\beta)D\left(-\alpha e^{i\frac{\pi}{2}\tilde{X}}\right)D(\beta)D\left(\alpha e^{i\frac{\pi}{2}\tilde{X}}\right)$ by choosing $|\alpha\beta| = \theta$.